THE JOURNAL OF PHYSICAL CHEMISTRY C

Article

Dielectric Properties of Organic Solvents in an Electrical Field

Isaak Nathan Daniels, Zhenxing Wang, and Brian Bostian Laird

J. Phys. Chem. C, **Just Accepted Manuscript** • DOI: 10.1021/acs.jpcc.6b10896 • Publication Date (Web): 15 Dec 2016

ACS Publications

The Journal of Physical Chemistry C is published by the American Chemical Society. 1155 Sixteenth Street N.W., Washington, DC 20036

Dielectric Properties of Organic Solvents in an Electrical Field

Isaak N. Daniels,[†] Zhenxing Wang,[†] and Brian B. Laird[*,†]

†*Department of Chemistry, University of Kansas, Lawrence, Kansas 66045, USA*

‡*Freiburg Institute for Advanced Studies, Albert Ludwigs Universität, Albertstraße 19, Freiburg, Germany*

E-mail: blaird@ku.edu

Abstract

The effect of an external electric field (E) on the dielectric constant (ε) of several pure solvents [propylene carbonate (PC), ethylene carbonate (EC), acetonitrile (MeCN) and dimethyl carbonate (DMC)] and for several EC/DMC mixtures is explored using classical molecular-dynamics simulation. Force fields were chosen that accurately predict the density and zero-field dielectric constant with respect to experiment. The simulation results for $\varepsilon(E)$ for field strengths up to 0.4 V/Å are calculated and fit to the Booth model, which is a standard functional form for the dependence of the dielectric constant on electric field. For PC and DMC, the Booth model gives an excellent representation of the data at all electric fields studied. For EC and MeCN, the Booth model works well at lower field strengths (up to 0.15 and 0.2 V/Å, respectively), but at the higher electric fields, these systems are observed to crystallize, a phenomenon referred to as *electrofreezing*. This work will provide useful input data for the continuum modeling of devices, such as electric double layer capacitors, that utilize organic electrolyte solvents.

Introduction

Research into the storage of renewable energy storage has become extremely important in recent years as a way to supplement and replace our dwindling supply of nonrenewable energy and reduce greenhouse gas emissions. Many important renewable energy sources, such as solar and wind, are intermittent; therefore, the development of robust and efficient energy storage is critical to ensure that energy is available when needed.

Energy storage devices vary in three main characteristics: energy density, power density and cycle life. Batteries, which store energy primarily through redox reactions, have high energy density, but have shortcomings with respect to power density and cycle life. Another class of systems, capacitors, which store energy through electrostatic interactions has high power density and cycle life, but low energy density. For many applications, a class of devices known as supercapacitors (referring to their very high

capacitance) has been successfully demonstrated to perform well with respect to all of these criteria. Two principal types of supercapacitors exist, electric double layer capacitors (EDLCs) and pseudocapacitors, in which the former is closer in concept to capacitors and the latter to batteries.

EDLCs consist of an electrolyte solution between two electrodes and are named for the electric "double layer" that is formed between the electrodes and the adjacent layers of ions in the electrolyte. In general, the energy stored in a capacitor at a fixed voltage difference can be estimated from the following equation

$$E = \frac{1}{2} C \left(\Delta V\right)^2 \tag{1}$$

where ΔV is the voltage difference between the electrodes and C is the capacitance of the system, which is proportional to the static (relative) dielectic constant of the electrolye, ε and the surface area of the electrode, but inversely proportional to the distance δ between the plates of the capacitor. In the case of EDLC's, δ is very small - on the order of the molecular diameter of the solvent. The small value of δ combined with high surface areas give EDLCs extremely large capacitances compared with other devices. For detailed continuum modeling of ELDCs, however, it is not enough to know the zero-field value of the solvent dielectric constant, as the local dielectric constant will depend upon other factors, such as the local electric field and the ion concentration. Experimentally, the electric field dependence of ε is difficult to measure, due in part to the limited field strengths achievable. Thus, atomistic computer simulations have been useful in providing this quantity for use as input for continuum models.[1–4]

In this work, we perform a series of molecular-dynamics (MD) simulations to determine the dielectric constant as a function of electric field for several, technologically relevant organic solvents. Organic electrolytes are often used in supercapacitor applications because they have a much higher electric potential threshold than water,[5,6] which puts a limit on the use of aqueous solutions. The data we obtain for $\varepsilon(E)$ for these systems are compared to a standard theoretical functional form, due to Booth[7,8]

and described in what follows.

Building on work by Onsager,[9] Booth[1,7,8] derived the following relation to model the dielectric constant of a solvent as a function of electric field:

$$\varepsilon_r = n^2 + \frac{3}{\tilde{\beta}E}[\varepsilon(0) - n^2]L(\tilde{\beta}E) \tag{2}$$

where E is the magnitude of the electric field, $\tilde{\beta}$ is a parameter, $\varepsilon(0)$ is the zero-field dielectric constant, n is the index of refraction (n^2 is equal to the infinite frequency dielectric constant,ε) and the Langevin function $L(x)$ is defined as

$$L(x) = \coth(x) - 1/x \tag{3}$$

(Note, earlier literature uses the symbol β for the Booth parameter. Here we use $\tilde{\beta}$ to distinguish it from $1/k_{\mathrm{B}}T$.) Using properties of water, Booth gave an estimate of $\tilde{\beta}$ in terms of the molecular dipole moment μ_e:

$$\tilde{\beta} = \frac{5\mu_e}{2k_{\mathrm{B}}T}\left(n^2 + 2\right) \tag{4}$$

where T is the absolute temperature and k_{B} is Boltzmann's constant Eq. 4 was derived specifically for water and its applicability for non-aqueous solvents has not been established. As a consequence, we treat $\tilde{\beta}$ as a fitting parameter for our data in this work.

Despite the importance of $\epsilon(E)$ in continuum simulations of electrode-electrolyte systems, simulation studies of this quantity for common electrolyte solvents are rare. Yeh and Berkowitz[10] used molecular-dynamics (MD) simulations to calculate the dielectric constant for water confined between Pt(111) electrodes for fields up to 0.4 V/Å. They found good agreement with the Booth equation using a model for $\tilde{\beta}$ found in Booth's original work,[7] using no fitted parameters. However, a corrected version of this equation[8] was found to be significantly worse.[11] Also using MD simulations, Yang, et al.[12] calculated the dielectric constant for the organic electrolyte propylene

carbonate (PC) as a function of electric field. Booth's equation (Eq. 2) was found to fit the data quite well with a reported best-fit value for $\tilde{\beta}^{-1} = 0.09$ V/nm. This corresponds to a $\tilde{\beta}$ of 11 nm/V, but as no error bars were reported, the statistical uncertainty in this value is unknown. The data from Ref. 12 was refit by Wang, et al.[4] obtaining a value of 13.14 for $\tilde{\beta}$(PC), which was then used by Varghese, et al.[3] as input for continuum modeling of PC/$LiClO_4$ EDLCs. In this same paper, ELDCs with acetonitrile/$LiCO_4$ electrolytes were also studied. Because simulation results for acetonitrile were not available, Varghese, et al. used Eq. 4 to estimate $\tilde{\beta}$ for acetonitrile, despite the fact that Eq. 4 was not derived for non-aqueous solvents.

In this work we have chosen four organic electrolytes for study: propylene carbonate (PC), ethylene carbonate (EC), dimethyl carbonate (DMC), and acetonitrile (MeCN). All of these solvents have been used in energy storage systems as either a pure solvent or mixed with another. These solvents possess dielectric constants that span almost two orders of magnitude. With our simulations, we can thus observe how the presence of an electric field affects solvents possessing quite different dielectric constants. Because the melting point of EC is higher than room temperature (36°C), it cannot be generally be used in its pure form, so for many applications it is often mixed with DMC to lower the melting point. Therefore, in addition to the pure solvent systems, we also examine mixtures of EC and DMC at various compositions. Of these solvents, only PC has received previous study (to our knowledge) using molecular simulation to determine $\varepsilon(E)$.[12] In addition to the dielectric constants and Booth equation fits, we also examine changes in the local structure - in the form of radial distribution functions - as a function of applied electric field.

Models and Methods

We model the organic solvents ethylene carbonate (EC), propylene carbonate (PC), dimethyl carbonate (DMC), acetonitrile (MeCN) and EC/DMC mixtures using a variety of force fields taken from the literature. These force fields consist of point charges

at atomic site and Lennard-Jones (LJ) 12-6 interactions for the non-bonded interactions (using standard Lorentz-Berthelot mixing rules). With a few exceptions outlined below, bond angles and bond lengths are held fixed (or nearly fixed using a high force constant), but dihedral angles (if applicable) are allowed to evolve under an appropriate dihedral potential. For the non-bonded LJ interactions, a polynomial switching function is applied between 10.0 Å and 10.1 Å to smoothly truncate the potential and forces. To calculate the electrostatic interactions, Particle-Particle Particle Mesh Ewald sums are used with a desired relative error of 10^{-6}.

For MeCN, we use the United Atom TraPPE force field of Wick, et al.[13] and bond lengths in MeCN are held fixed using the SHAKE algorithm.[14] For DMC, we base our interactions on the united atom force field used by Wheeler,[15] which was adapted from the OPLS-UA parameter set[16] to study diffusion in organic electrolytes. Our force field is identical to that of Wheeler with two exceptions: First, Wheeler applies a scaling factor to the 1-5 carbon-carbon intramolecular LJ interaction, whereas we use the full interaction. Second, we use Lorentz-Berthelot mixing rules for LJ interactions instead of the modified mixing rules used by Wheeler. With the exception of the dihedral angle, all bond angles and bond lengths are held (nearly) rigid in the simulations through the use of very high force constants for those degrees of freedom. These modifications for DMC improve the value of the zero-field dielectric constant at 298K from 1.63(2)[15] to 2.49(2) (the experimental value is 3.20),[17] without substantially affecting other properties, such as the density. Here, and in what follows, the numbers in parentheses represent the statistical error (95% confidence level) for the last digit(s) shown.

The LJ interactions for EC and PC are taken from Cornell's Amber parm94 force field,[18] including explicit hydrogens. The charges on the atoms we use are those of Arslanargin, et al.[19] and Yang, et al.[12] for EC and PC, respectively. For EC and PC all bond angles and bond lengths are (nearly) fixed by using a high force constant for these degrees of freedom, with the exceptions of the bond angles in PC centered at the methyl carbon.

All molecular-dynamics (MD) simulations were performed using the molecular sim-

ulation code LAMMPS,[20] with a time step of 1 fs. Initial liquid configurations for all solvents were generated using the program Packmol.[21] The equilibrium densities for these solvents at 1 atm pressure were determined using isothermal-isobaric (constant NPT) MD simulations using a Nosé-Hoover thermostat and an Anderson barostat. For MeCN and PC, we used a temperature of 298 K; however, because of the high melting point of EC, 313.0 K was used for the pure EC simulations as well as for the EC/DMC mixtures (including pure DMC). The damping parameters for both the thermostat and barostat were set to 100 fs, with the exception of the simulations for MeCN where the barostat damping parameter was set to 500 fs because of numerical instabilities encountered with the lower value. Production runs to determine the dielectric constant under an applied electric field were performed using isothermal (constant NVT) MD simulations using a Nosé-Hoover thermostat (100 fs damping parameter). The initial configurations for the NVT simulations were obtained by choosing configurations from the equilibrium NPT simulations for which the instantaneous volume was equal to the average volume of the NPT run. The NVT simulations were equilibrated for a minimum of 10 ns followed by runs of 30 to 110 ns for collecting averages. As in the simulations of the electric field dependence of the dielectric constant of PC by Yang, et al.[12] we simulate our systems at various electric fields ranging from 0 to 4 V/nm.

In our simulations, the dielectric constant was determined from the fluctuations in total dipole moment according to the relation[22]

$$\varepsilon = n^2 + \frac{\left\langle M^2 \right\rangle - \langle M \rangle^2}{3Vk_BT\varepsilon_0} \tag{5}$$

where M is the total instantaneous dipole moment of the simulation box and ε_0 is the permittivity of the vacuum. For classical simulations with non-polarizable force fields, such as this work, $n^2 = \varepsilon_\infty$ is assumed to be 1 because of the lack of electronic degrees of freedom in the model. Coordinates were sampled every 1 ps during the simulation to calculate $\left\langle M^2 \right\rangle$ and $\langle M \rangle^2$.

Results

Verification of force fields

To verify the force fields used, we have calculated the equilibrium densities and zero-field dielectric constants for both the pure and mixed solvents and compared them to experiment. The equilibrium densities at 1 atm pressure from both simulation and experiment for the pure solvents are shown in Table 1. All densities were evaluated at 298 K, except for EC which was evaluated at 313 K to be above the melting point. From this comparison we see that the densities of the pure solvents are in good to excellent agreement with experiment.

Table 1: Densities of organic electrolyte solvents from simulation

Solvent	**Temperature**	**Density** (g/mL) *Experiment*	**Density (g/mL)** *Simulation*
EC	313 K	1.32199[17]	1.3241(9)
PC	298 K	1.1976[24]	1.2245(9)
MeCN	298 K	0.7762[25]	0.7828(6)
DMC	298 K	1.06350[26]	1.0549(14)
DMC	313 K	1.041800[17]	1.0349(15)

For the EC/DMC mixtures, the equilibrium densities as a function of the mole fraction of EC at 313 K and 1 atm pressure are shown in Fig. 1. As was seen for the pure systems, the agreement between simulation and experiment is very good.

The dielectric constants at zero-field for the pure solvents were calculated and are shown in Table 2 along with the reported experimental values from the literature. The agreement between simulation and experiment is good with a maximum deviation of about 18% for EC and 25% in the case of DMC. For the case of DMC, this discrepancy can be explained by the fact that, in the simulations, the index of refraction n (and the corresponding value of the high-frequency dielectric constant $\varepsilon_\infty = n^2$) is assumed to be equal to 1 when determining the dielectric constant from Eq. 5. Typically, n is between 1 and 2, so for solvents such as EC, PC and MeCN which have large static dielectric constants, the setting of n to 1 has minimal effect. For DMC, however, which

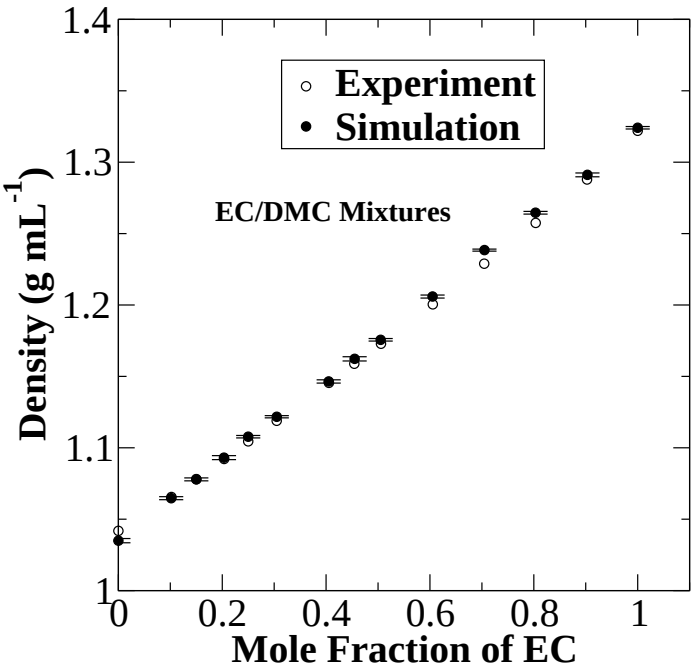

Figure 1: Density of EC/DMC mixtures at 313 K and 1 atm pressure as a function of the mole fraction of EC for both simulation and experiment.[17]

has a low static dielectric constant, $n^2 = \varepsilon_\infty$ makes substantial contribution to ε. If one uses the DMC experimental value $(1.370)^{23}$ for n for DMC in Eq. 5, one obtains a value of 3.21, which is almost identical with the experimental value listed in Table 2. Therefore, the model describes well describes the contribution of dipole fluctuations to the dielectric constant. Note that, in fitting the data to the Booth model (Eq. 2) one first subtracts n^2 from $\varepsilon(E)$, so the Booth model fits should be unaffected by the approximation that $n^2 = 1$ in these non-polarizable classical simulations.

The zero-field relative dielectric constants for the EC/DMC mixtures from both experiment and simulation are shown in Fig. 2 as a function of EC mole fraction at 313 K and 1 atm pressure. Except for the very highest EC mole fractions, the agreement between experiment and simulation is excellent. The agreement between experimental and simulated values of the density and zero-field dielectric constants for the pure and mixed organic electrolyte solvents studied here give us confidence that the force fields

Table 2: Zero-field dielectric constants for pure solvents from simulation and experiment.

Solvent	Temperature	Dielectric Constant	Dielectric Constant
		Experiment	*Simulation*
EC	313 K	90.03[17]	106(6)
PC	298 K	64.92[27]	61(4)
MeCN	298 K	35.95[28]	32.7(4)
DMC	298 K	3.20[17]	2.49(2)
DMC	313 K	3.10-3.19[17]	2.340(14)

chosen accurately represent the systems chosen for study.

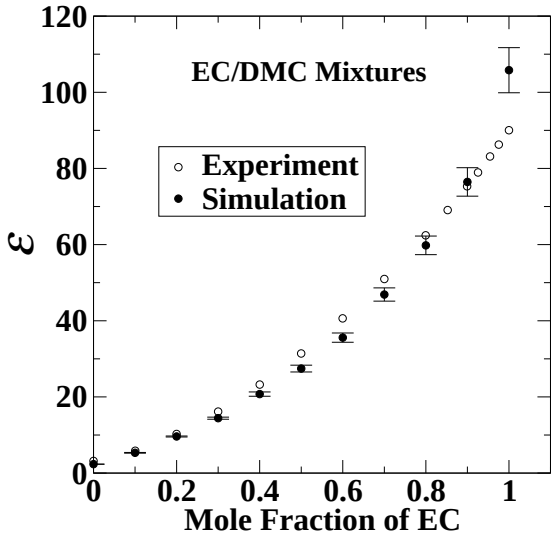

Figure 2: Dielectric constant of EC/DMC mixtures at 313 K and 1 atm as a function of EC mole fraction. Experimental data from Ref. 17 is shown for comparison.

Dielectric constant as a function of electric field

With the force fields validated we turn our attention to the effect of electric field on the relative dielectric constant of pure and mixed organic solvents. The dielectric constants for pure MeCN, EC, PC and DMC as a function of applied electric fields up to 0.4 V/Å are shown in Fig. 3 at 298 K (for MeCN and PC) and 313 K (for EC and DMC). (Because we will also be studying mixtures of EC and DMC at 313K (to be above the

melting point of pure EC), both the pure EC and DMC systems were also studied at this temperature.) As expected, the presence of the electric field lowers the dielectric constant significantly. Increasing the electric field constrains the rotation of the dipoles and makes them less able to screen the interaction between ions in the electrolyte. At the highest fields we see that the dipole orientation becomes saturated - that is, become highly aligned with the field - and the relative dielectric constant tends to the vacuum value of 1. For MeCN and EC, we observe anomalously low values of the dielectric constant at very high fields (starting about 0.15 V/Å for EC and 0.3 V/Å for MeCN). Detailed analysis of the structure (discussed in the next section) of the solvent indicates that these low values are due to the crystallization of the solvent at high field. The crystallization of polar fluids under high fields is often referred to *electrofreezing* and has been observed earlier in molecular simulations of water.[29]

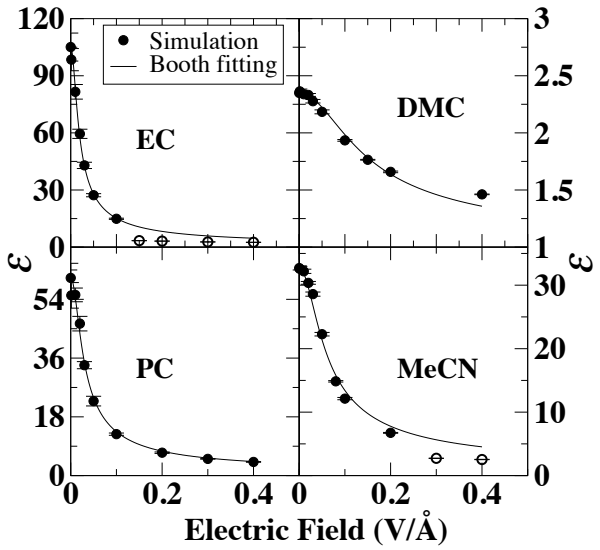

Figure 3: Dielectric constant as a function of external electric field calculated from MD simulation (symbols) on several pure organic solvents at 298 K (PC and MeCN) and 313K (EC and DMC). The solid lines denote fits to the Booth Model (Eq. 2). The open symbols denote data points where the solvent was observed to crystallize (electrofreezing). These points were excluded from the Booth-Model fitting.

Also shown in Fig. 3 are the results of non-linear least squares fits to the Booth model (Eq. 2) for the pure solvents studied. For these Booth Model fittings, the anomalously low values of ε due to crystallization were excluded. The best-fit values

of $\tilde{\beta}$ are shown in Table 3. In this table, the $\tilde{\beta}$ value for DMC at 313 K is also shown.

Table 3: Values of $\tilde{\beta}$ from Booth model fits of the simulation data for the pure solvents.

System	Temperature	$\tilde{\beta}$ (nm/V)
PC	298 K	13.3(18)
MeCN	298 K	6.48(15)
DMC	313 K	2.55(6)
EC	313 K	21(2)

From the data in Tables 2 and 3 we observe that the higher values of $\varepsilon(E = 0)$ correspond to higher values of $\tilde{\beta}$, that is, higher values of the zero-field dielectric constant (and higher molecular dipole moments) lead to significantly faster decrease in ε with increasing field. This is consistent with Booth's Eq. 4 in which $\tilde{\beta}$ is predicted to be proportional to the magnitude of the dipole moment. While the pre-factor in Eq. 4 is not appropriate for non-aqueous solutions, the general dependence of $\tilde{\beta}$ on the dielectric constant should still be valid. For PC, we see reasonable agreement of our $\tilde{\beta}$ value of 13.3(18) nm/V with the value of 13.14 nm/V obtained in the earlier simulations of Wang, et al.[4] There is a slight discrepancy between the two values for PC, but exact comparisons are difficult because the value obtained in Ref. 4 was at a slightly different temperature than our results (300 K versus 298 K, respectively) and no error bars are given in Ref. 4. It is useful to note that for MeCN, our value of $\tilde{\beta} = 6.48(15)$ nm/V is considerably smaller than the one used (30.15 nm/V) in Refs. 3 and 4 as input for continuum model simulations for MeCN-based EDLCs. In that work, Eq. 4 was used to determine a value of $\tilde{\beta}$ for MeCN. This discrepancy illustrates the danger of the general use of Eq. 4 as this equation for $\tilde{\beta}$ was derived using structural properties of aqueous solutions and should not be applied to non-aqueous solvents, such as MeCN. It is interesting to note that the Booth Model functional form works well for DMC, despite the fact that the Booth Model was derived assuming that the zero-field static dielectric constant (ε) is much greater than the high-frequency dielectric constant ($\varepsilon_\infty = n^2$), which is clearly not the case for DMC as its value $\varepsilon(E = 0)$ is not

much greater than 1.

The dielectric constants as a function of electric field for various EC/DMC mixtures are shown in Fig. 4. These data were taken at 313 K (above the melting point of EC) and 1 atm pressure in order to be able to examine the full range of compositions. For mixtures with high EC content (EC mole fraction of 0.7 or above), crystalization (electrofreezing) was observed to occur at high electric fields. After excluding the points for which electrofreezing occurred at high field strength and high EC mole fraction, the data in Fig 4 were fit to the Booth model using non-linear least squares regression. The resulting values are shown in Table 4. As was seen in the case of the pure solvents, the value of $\tilde{\beta}$ decreases with decreasing ε.

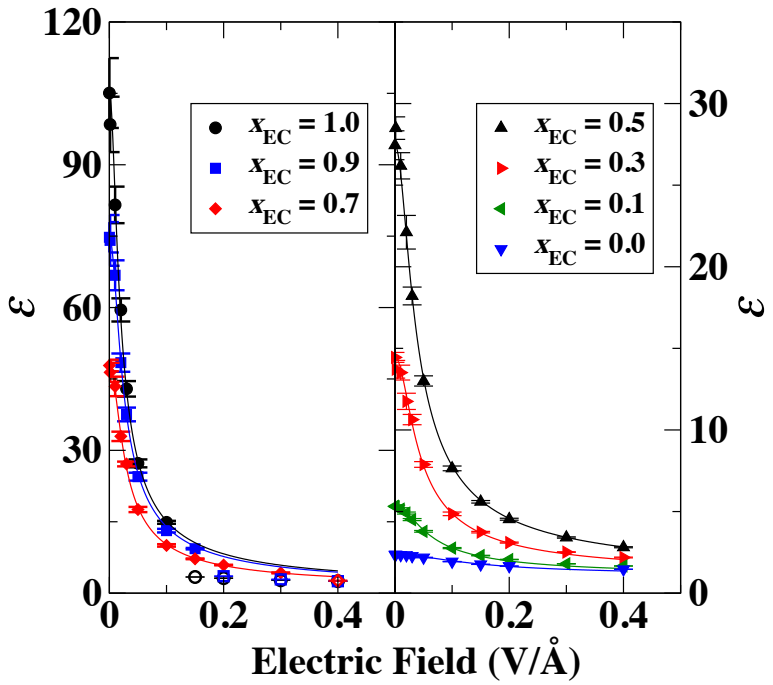

Figure 4: Dielectric constant for various compositions of EC/DMC mixtures as a functions of external electric field calculated from MD simulation (symbols) on several pure organic solvents. The solid lines denote fits to the Booth Model (Eq. 2). The open symbols denote data points where the solvent was observed to crystallize (electrofreezing'). These points were excluded from the Booth-Model fitting.

Table 4: Fitted values of $\tilde{\beta}$ for EC/DMC solvents from simulation

EC mole fraction (x_{EC})	$\tilde{\beta}$(nm/V)Fitted Value
1.00	21(2)
0.90	16.0(8)
0.70	14.1(7)
0.50	10.6(5)
0.30	9.3(5)
0.10	6.1(2)
0.00	2.55(6)

Electrofreezing of EC, MeCN and EC/DMC mixtures at high electric field

In Figs. 3 and 4 we observed, at high electric field, anomalously low values of the dielectric constant in EC, MeCN and EC/DMC mixtures with high EC content. These low values correspond to solvents that have crystallized (electrofreezing) in the presence of the field. The hindered molecular rotation in these crystals dramatically lowers the ability of the system to respond to an external field - yielding a reduced dielectric constant. To illustrate the crystallization, snapshot images (produced using the molecular imaging program VMD[30]) for pure EC at 0.1 V/Å and 0.15 V/Å are shown in Fig. 5. At the lower field (0.1 V/Å), the system is still fluid, however, as the field is raised to 0.15 V/Å, distinct layers consistent with crystallization are seen to form. Although the force field used for EC describes the liquid phase reasonably well, the crystal phase equilibrium properties of this force field have not been studied and it is not known if the lowest free energy crystal phase of this model conforms to the known EC crystal structure. Therefore, we have not characterized the crystal structure formed here by electrofreezing, because in the absence of experimental confirmation it is difficult to assess the validity of the structure. Unfortunately, the electrofreezing predicted here occurs at field strengths for which it is difficult to perform experiments. However, electrofreezing has been observed for water at much smaller fields when confined to a small volume,[31] so it may be possible to examine this more closely in the future.

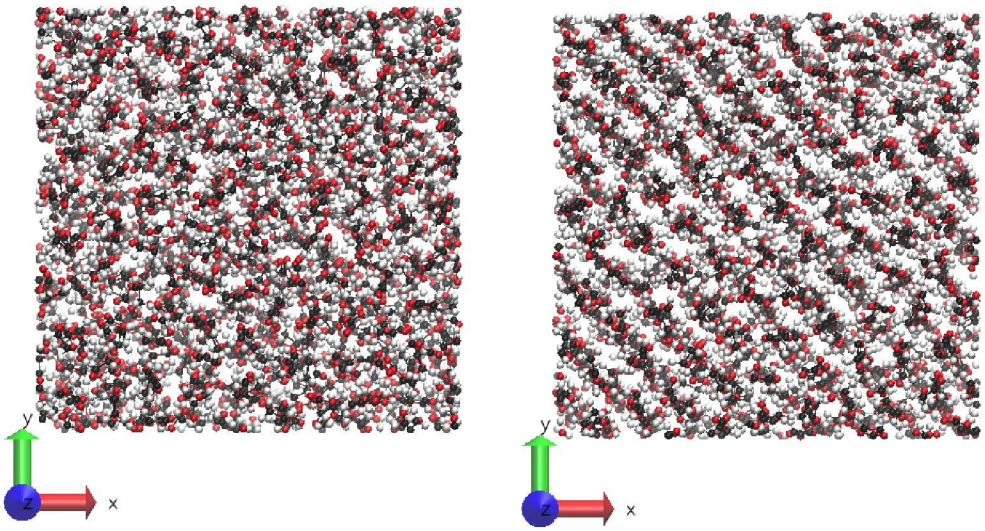

Figure 5: Snapshots from the simulation of pure EC at electric fields of 0.1 V/Å(left) and 0.15 V/Å(right)

The electrofreezing in the EC/DMC mixtures can also be examined using radial distribution functions (RDFs). As a proxy for the molecular center, we examine the RDFs between the carbonyl oxygens (O_C) on different EC molecules. The RDFs for EC/DMC mixtures with selected EC mole fractions of 1.0, 0.9, 0.7 and 0.5 are shown in Fig. 6. (RDFs at other values of the EC mole fractions are included in the Supporting Information.) For an equimolar EC/DMC solution ($x_{EC} = 0.5$), the liquid structure changes continuously as the electric field is increased - no evidence of discontinuous structural change is seen. However, when the solution reaches a 0.7 mole fraction of EC a discontinuous change in structure corresponding to electrofreezing of the solvent is observed to take place between field strengths of 0.3 V/Å and 0.4 V/Å. As the EC mole fraction is further increased to 0.9 and 1.0, the electrofreezing transition is shifted to lower values of the electric field magnitude. As the EC mole fraction decreases from 1, the solvent moves further away from the melting point and deeper into the liquid phase requiring more energy to stabilize a crystalline orientationaly ordered form.

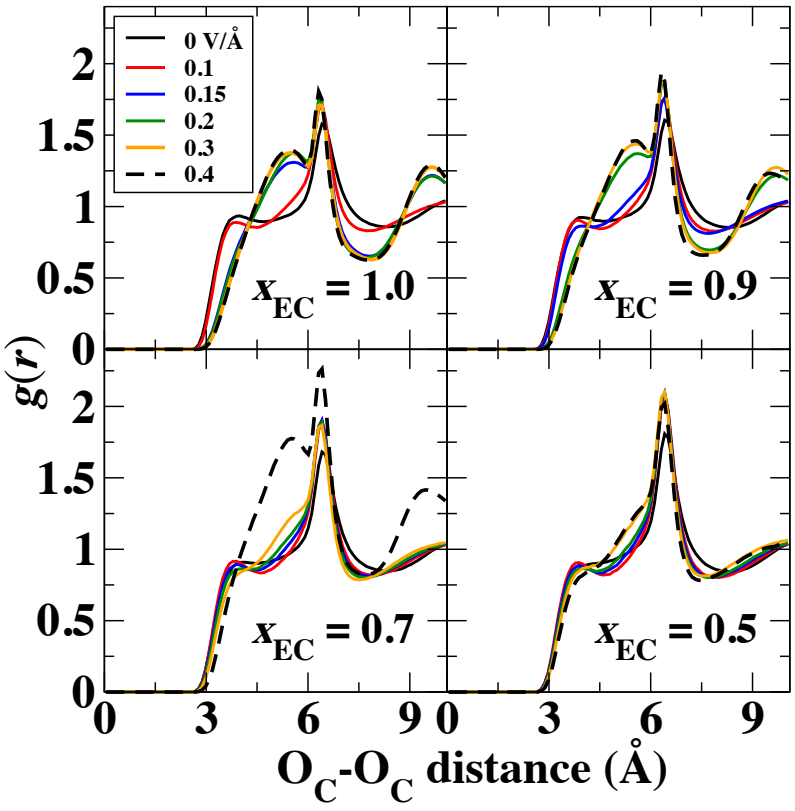

Figure 6: RDFs (O_C-O_C) for EC/DMC mixtures with EC mole fractions of 1.0, 0.9, 0.7 and 0.5 at 313 K and 1 atm pressure at a variety of electric field values

From our simulations, we also examine the degree to which the molecules orient with respect to the electric field direction as the electric field is increased. To quantify this, we calculated the average of the cosine of the angle between the molecular dipole moment unit vector $\hat{\mu}$ and the unit vector corresponding to the electric field direction $\hat{e}$.

$$\langle \cos\theta \rangle = \langle \cos \hat{\mu} \cdot \hat{e} \rangle \tag{6}$$

In Fig. 7, we plot the quantity $\langle 1 - \cos\theta \rangle$ as a function of the electric field. As was seen in the case of the dielectric constant, $\langle 1 - \cos\theta \rangle$ decreases rapidly as the electric field is increased with solvents with higher zero-field dielectric constant showing the fastest rate of decline. One can compare these curves to that predicted from statistical mechanics

for a system of noninteracting polar molecules with dipole moment magnitude, μ:

$$\langle 1 - \cos\theta \rangle = 1 - L(\beta\mu E) \tag{7}$$

where $L(x)$ is the Langevin function defined in Eq. 3 and $\beta = 1/k_{\mathrm{B}}T$. Note the similarity of this form to that of the Booth model (Eq. 2). Because the polar solvents here are fluid and have considerable intermolecular interactions, Eq. 7 is not expected to fit the data directly as is, but it does provide a useful functional form to model the data by allowing $\mu^* = \beta\mu$ to be an adjustable parameter. The non-linear least squares fits to Eq. 7 for all pure solvents are also shown in Fig. 7. (The specific values of the effective reduced dipole moment μ^* for these fits can be found in the Supporting Information) Although derived for non-interacting dipoles, Eq. 7 used as a fitting functional form provides an excellent model for the data.

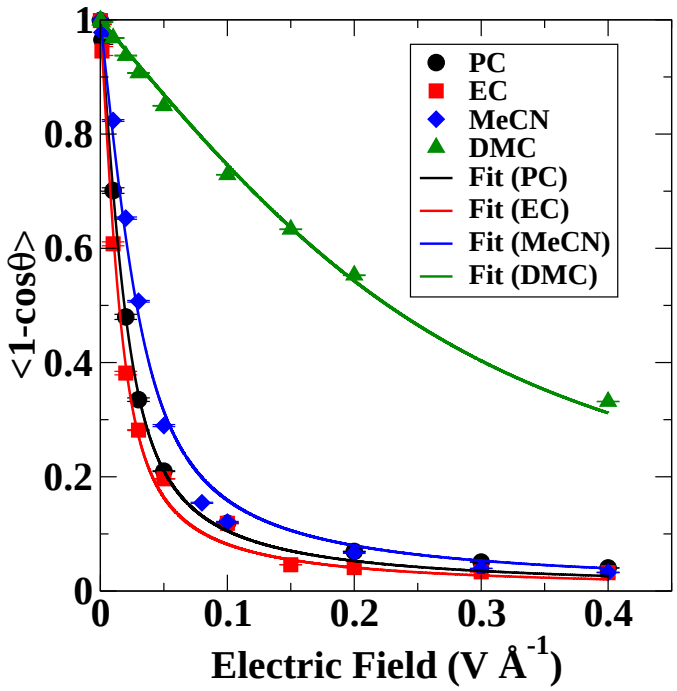

Figure 7: Simulation values of $\langle 1 - \cos\theta \rangle$ as a function electric field for all pure solvents studied. The solid lines are the result of a fit to Eq. 7 using $\mu^* = \beta\mu$ as an adjustable parameter.

Summary

Using molecular-dynamics (MD) simulation, we have calculated the dependence of the relative dielectric constant, ε, on the magnitude of the applied electric field, E, for several polar solvents: ethylene carbonate (EC), propylene carbonate (PC), acetonitrile (MeCN), dimethyl carbonate (DMC) and several EC/DMC mixtures of varying composition. The set of solvents have zero-field dielectric constants that span from 3 to nearly 100. All of these non-aqueous solvents have been used as electrolyte solvents in battery and supercapacitor applications as they have a higher stability range with respect to electric field strength than aqueous electrolytes. The dependence of the dielectric constant on the external electric field is difficult to measure experimentally - especially at high field strengths - but is an important input quantity for continuum modeling of electric double layer capacitors (EDLCs) and other energy storage devices.[1–4] The force fields used in this study give good to excellent agreement with experimental values of the solvent density and zero-field dielectric constant for the solvents studied.

As expected, the dielectric constant for each of the solvents studied decreases rapidly with increasing electric field (up to 0.4 V/Å). The rate of decrease correlates significantly with the zero-field dielectric constant, as well as with the dipole moment of the solvent molecules. For EC, MeCN and EC/DMC mixtures with high EC mole fraction, the solvents were observed to crystallize at sufficiently high electric fields - a phenomenon known as *electrofreezing* that has been observed previously in simulations of water.[29] The nature of the discontinuous freezing transition was examined structurally using visual analysis of sample configurations and analysis of radial distribution functions (RDFs). The simulation data is found to be fit very well by a functional form due to Booth[1,7,8] (Eq. 2) using Booth's parameter $\tilde{\beta}$ as a fitting parameter. Data points corresponding to systems that have crystallized (electrofreezing) were excluded from the fits. These Booth model fits should provide convenient analytical forms for $\epsilon_r(E)$ for use in continuum models. The value of $\tilde{\beta}$ obtained for PC

was in good agreement with a previous MD simulation result using a slightly different potential.[4]

In the original derivations of Eq. 2, Booth provided an expression for $\tilde{\beta}$ (Eq. 4) that can be evaluated directly from the magnitude of the molecular dipole moment and the index of refraction; however, the derivation of this expression incorporates structural properties of water and the use of this equation for non-aqueous solvents is not advised. For example, using Eq. 4 for MeCN at 298 K yields a value of 30.15 nm/V for $\tilde{\beta}$,[3,4] that is over four times larger than the simulation prediction of 6.48(0.15). These calculations show that the use of Eq. 4 for nonaqueous solvents should be avoided. Because of the difficulty in obtaining experimental values for the dependence of the dielectric constant on electric field, the data presented should prove useful as input for future continuum modeling of electric storage devices.

Supporting Information Available

A document containing Supporting Information for this work is available for the interested reader. Included are tables listing the numerical values for the data presented in Figs. 1 and 4 and additional radial distribution functions for EC mole fractions not shown in Fig. 6. Also included in the Supporting Information is a table of the effective dielectric constants, μ^* from the fits used to create Fig. 7. This material is available free of charge via the Internet at `http://pubs.acs.org/`.

Acknowledgement

This work was supported in part by the Center for Molecularly Engineered Energy Materials, an Energy Frontier Research Center funded by the US Department of Energy, Office of Science, Office of Basic Energy Sciences under Award No. DE-SC0001342. BBL also wishes to thank the Freiburg Institute for Advanced Studies in Freiburg, Germany for hosting him during the completion of this work.

References

(1) Gur, Y.; Ravina, I.; Babchin, A. J. On the electrical double layer theory. II. The Poisson—Boltzmann equation including hydration forces. *J. Colloid Interface Sci.* **1978**, *64*, 333–341.

(2) Wang, H.; Pilon, L. Accurate simulations of electric double layer capacitance of ultramicroelectrodes. *J. Phys. Chem. C* **2011**, *115*, 16711–16719.

(3) Varghese, J.; Wang, H.; Pilon, L. Simulating electric double layer capacitance of mesoporous electrodes with cylindrical pores. *J. Electrochem. Soc.* **2011**, *158*, A1106–A1114.

(4) Wang, H.; Varghese, J.; Pilon, L. Simulation of electric double layer capacitors with mesoporous electrodes: Effects of morphology and electrolyte permittivity. *Electrochim. Acta* **2011**, *56*, 6189–6197.

(5) Hall, P. J.; Mirzaeian, M.; Fletcher, S. I.; Sillars, F. B.; Rennie, A. J.; Shitta-Bey, G. O.; Wilson, G.; Cruden, A.; Carter, R. Energy storage in electrochemical capacitors: designing functional materials to improve performance. *Energ. Environ. Sci.* **2010**, *3*, 1238–1251.

(6) Winter, M.; Brodd, R. J. What are batteries, fuel cells, and supercapacitors? *Chem. Rev.* **2004**, *104*, 4245–4270.

(7) Booth, F. The dielectric constant of water and the saturation effect. *J. Chem. Phys.* **1951**, *19*, 391–394.

(8) Booth, F. Errata: the dielectric constant of water and the saturation effect. *J. Chem. Phys.* **1951**, *19*, 1327–1328.

(9) Onsager, L. Electric moments of molecules in liquids. *J. Am. Chem. Soc.* **1936**, *58*, 1486–1493.

(10) Yeh, I.-C.; Berkowitz, M. L. Dielectric constant of water at high electric fields: molecular dynamics study. *J. Chem. Phys.* **1999**, *110*, 7935–7942.

(11) Fulton, R. L. The nonlinear dielectric behavior of water: Comparisons of various approaches to the nonlinear dielectric increment. *J. Chem. Phys.* **2009**, *20*, 204503.

(12) Yang, L.; Fishbine, B. H.; Migliori, A.; Pratt, L. R. Dielectric saturation of liquid propylene carbonate in electrical energy storage applications. *J. Chem. Phys.* **2010**, *132*, 044701.

(13) Wick, C. D.; Stubbs, J. M.; Rai, N.; Siepmann, J. I. Transferable potentials for phase equilibria. 7. Primary, secondary and tertiary amines, nitroalkanes and nitrobenzenes, nitriles, amides, pyridine, and pyrimidine. *J. Phys. Chem. B* **2005**, *109*, 18974–18982.

(14) Ryckaert, J.-P.; Ciccotti, G.; Berendsen, H. J. C., *J of Comp. Phys.*, **1977**, *23*, 327–341..

(15) Wheeler, D. R. Molecular simulations of diffusion in electrolytes. Ph.D. thesis, University of California, Berkeley, 2002.

(16) Jorgensen, W. L.; Tirado-Rives, J. The OPLS [optimized potentials for liquid simulations] potential functions for proteins, energy minimizations for crystals of cyclic peptides and crambin. *J. Amer. Chem. Soc.* **1988**, *110*, 1657–1666.

(17) Naejus, R.; Lemordant, D.; Coudert, R.; Willman, P. Excess thermodynamic properties of binary mixtures containing linear or cyclic carbonates as solvents at the temperatures 298.15 K and 313.15 K. *J. Chem. Thermodyn.* **1997**, *29*, 1503–1515.

(18) Cornell, W. D.; Cieplak, P.; Bayly, C. I.; Gould, I. R.; Merz, K. M.; Ferguson, D. M.; Spellmeyer, D. C.; Fox, T.; Caldwell, J. W.; Kollman, P. A. A second

generation force field for the simulation of proteins, nucleic acids and organic molecules. *J. Am. Chem. Phys.* **1995**, *117*, 5179–5197.

(19) Arslanargin, A.; Powers, A.; Beck, T. L.; Rick, S. W. Models of ion solvation thermodynamics in ethylene carbonate and propylene carbonate. *J. Phys. Chem. B* **2015**, *120*, 1497–1508.

(20) Plimpton, S. Fast parallel algorithms for short-range molecular dynamics. *J. Comp. Phys.* **1995**, *117*, 1–19.

(21) Martínez, L.; Andrade, R.; Birgin, E. G.; Martínez, J. M. Packmol: A package for building initial configurations for molecular dynamics simulations. *J. Comp. Chem.* **2009**, *30*, 2157–2164.

(22) Neumann, M. Dipole moment fluctuation formulas in computer simulations of polar systems. *Mol. Phys.* **1983**, *50*, 841–858.

(23) Moosavi, M.; Motahari, A.; Vahid, A.; Akbar, V.; Rostami, A. A.; Obrani, A. Densities, Viscosities, and Refractive Indices of Dimethyl Carbonate + 1-Hexanol/1-Octanol Binary Mixtures at Different Temperatures. *J. Chem. Eng. Data* **2016**, *61*, 1981-1991.

(24) Arbad, B. R.; Lande, M. K.; Wankhede, N. N.; Wankhede, D. S. Viscosities, ultrasonic velocities at (288.15 and 298.15) K, and refractive indices at (298.15) K of binary mixtures of 2, 4, 6-trimethyl-1, 3, 5-trioxane with dimethyl carbonate, diethyl carbonate, and propylene carbonate. *J. Chem. Eng. Data* **2006**, *51*, 68–72.

(25) Nikam, P. S.; Shirsat, L. N.; Hasan, M. Density and viscosity studies of binary mixtures of acetonitrile with methanol, ethanol, propan-1-ol, propan-2-ol, butan-1-ol, 2-methylpropan-1-ol, and 2-methylpropan-2-ol at (298.15, 303.15, 308.15, and 313.15) K. *J. Chem. Eng. Data* **1998**, *43*, 732–737.

(26) Garcia de la Fuente, I.; Gonzalez, J. A.; Cobos, J. C.; Casanova, C. Excess molar volumes for dimethyl carbonate+ heptane, decane, 2, 2, 4-trimethylpentane, cy-

clohexane, benzene, toluene, or tetrachloromethane. *J. Chem. Eng. Data* **1992**, *37*, 535–537.

(27) Payne, R.; Theodorou, I. E. Dielectric properties and relaxation in ethylene carbonate and propylene carbonate. *J. Phys. Chem.* **1972**, *76*, 2892–2900.

(28) Cunningham, G. P.; Vidulich, G. A.; Kay, R. L. Several properties of acetonitrile-water, acetonitrile-methanol, and ethylene carbonate-water systems. *J. Chem. Eng. Data* **1967**, *12*, 336–337.

(29) Svishchev, I. M.; Kusalik, P. G. Crystallization of liquid water in a molecular dynamics simulation. *Phys. Rev. Lett.* **1994**, *73*, 975.

(30) Humphrey, W.; Dalke, A.; Schulten, K. Visual molecular dynamics. *J. Molec. Graphics* **1996**, *14*, 33–38.

(31) Choi, E.-M.; Yoon, Y.-H.; Lee, S.; Kang, H. Freezing transition of interfacial water at room temperature under electric fields. *Phys. Rev. Lett.* **2005**, *95*, 085701.

Table of Contents Figure

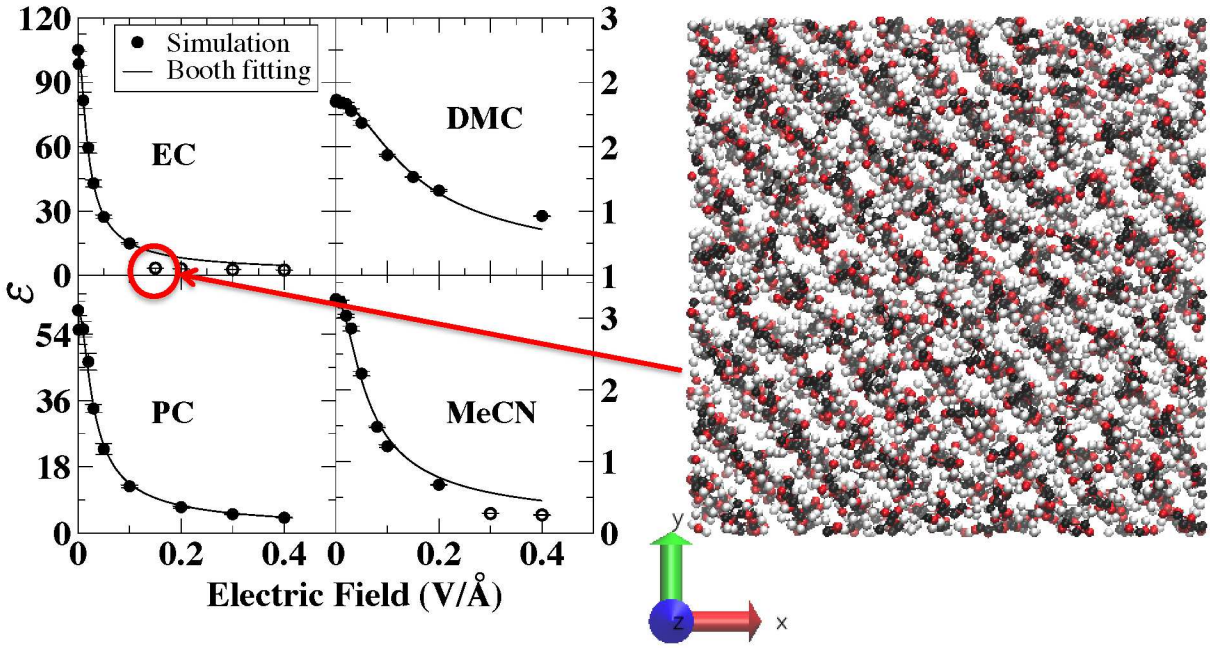

Figure 8: Table of Contents Figure